Cell

Implications for Kinetochore-Microtubule Attachment from the Structure of an Engineered Ndc80 Complex

Claudio Ciferri,[1,8,10] Sebastiano Pasqualato,[1,8] Emanuela Screpanti,[1] Gianluca Varetti,[1,9] Stefano Santaguida,[1,9] Gabriel Dos Reis,[1] Alessio Maiolica,[1] Jessica Polka,[2] Jennifer G. De Luca,[3] Peter De Wulf,[1] Mogjiborahman Salek,[4] Juri Rappsilber,[5] Carolyn A. Moores,[6] Edward D. Salmon,[2] and Andrea Musacchio[1,7,*]

[1]Department of Experimental Oncology, European Institute of Oncology, Via Adamello 16, I 20139 Milan, Italy
[2]Department of Biology, University of North Carolina, Chapel Hill, NC 27599-3280, USA
[3]Department of Biochemistry and Molecular Biology, Colorado State University, Fort Collins, CO 80523-1870, USA
[4]Sir William Dunn Pathology School, South Parks Rd, Oxford, OX1 3RE, UK
[5]Wellcome Trust Centre for Cell Biology, University of Edinburgh, Edinburgh EH9 3JR, UK
[6]School of Crystallography, Birkbeck College, University of London, London WC1E 7HX, UK
[7]Research Unit of the Italian Institute of Technology (IIT) Foundation at the IFOM-IEO Campus, Via Adamello 16, I-20139 Milan, Italy
[8]These authors contributed equally to this work.
[9]These authors contributed equally to this work.
[10]Present address: Department of Molecular and Cell Biology, University of California, Berkeley, CA 94720, USA.
*Correspondence: andrea.musacchio@ifom-ieo-campus.it
DOI 10.1016/j.cell.2008.03.020

SUMMARY

Kinetochores are proteinaceous assemblies that mediate the interaction of chromosomes with the mitotic spindle. The 180 kDa Ndc80 complex is a direct point of contact between kinetochores and microtubules. Its four subunits contain coiled coils and form an elongated rod structure with functional globular domains at either end. We crystallized an engineered "bonsai" Ndc80 complex containing a shortened rod domain but retaining the globular domains required for kinetochore localization and microtubule binding. The structure reveals a microtubule-binding interface containing a pair of tightly interacting calponin-homology (CH) domains with a previously unknown arrangement. The interaction with microtubules is cooperative and predominantly electrostatic. It involves positive charges in the CH domains and in the N-terminal tail of the Ndc80 subunit and negative charges in tubulin C-terminal tails and is regulated by the Aurora B kinase. We discuss our results with reference to current models of kinetochore-microtubule attachment and centromere organization.

INTRODUCTION

The mitotic spindle, a microtubule-based scaffold, captures, aligns, and separates the replicated chromosomes (sister chromatids) during mitosis (O'Connell and Khodjakov, 2007). The spindle assembly checkpoint detects defects in chromosome-spindle attachment and delays anaphase to prevent errors in chromosome segregation. These errors generate imbalances in chromosome numbers that are frequently observed in cancer cells (Musacchio and Salmon, 2007).

Stable chromosome-spindle attachments are formed through kinetochores, scaffolds of ~100 different proteins assembled at the periphery of centromeric DNA nucleosomes containing the histone H3 variant CENP-A (Cleveland et al., 2003; Maiato et al., 2004). *Saccharomyces cerevisiae* has compact kinetochores that attach to a single microtubule (Cleveland et al., 2003; Joglekar et al., 2006; McAinsh et al., 2003; Meraldi et al., 2006; Tanaka et al., 2005). Most eukaryotes assemble larger kinetochores with multiple attachment sites (15–30) for the plus ends of spindle microtubules, which are organized in kinetochore fibers (Cleveland et al., 2003). At low resolution, the kinetochore of vertebrates appears as a trilaminar disk, with an electron-dense inner plate at the periphery of centromeric chromatin, an electron-lucent middle layer, and an electron-dense outer plate, the site of end-on binding of microtubule plus ends (Cleveland et al., 2003). Electron tomography-based reconstructions of the outer plate revealed a fibrous structure that undergoes significant reorganization upon end-on microtubule attachment (Dong et al., 2007).

The Ndc80 complex is a core component of the end-on attachment sites for kinetochore microtubules (Ciferri et al., 2007; Kline-Smith et al., 2005). Its depletion perturbs the architecture of the kinetochore outer plate and reduces the number of attached microtubules (DeLuca et al., 2005; Liu et al., 2006). The four subunits of the Ndc80 complex, named Ndc80 (human Ndc80 is also known as Hec1, for *h*ighly *e*xpressed in *c*ancer *1*), Nuf2, Spc24, and Spc25, assemble into a 170–190 kDa complex in different species (Ciferri et al., 2007; Kline-Smith et al., 2005; Maiato et al., 2004). All four subunits contain long coiled coils (Figure S1 available online). Low-resolution structural analyses of yeast and human Ndc80 complexes (Ciferri et al., 2005; Wei

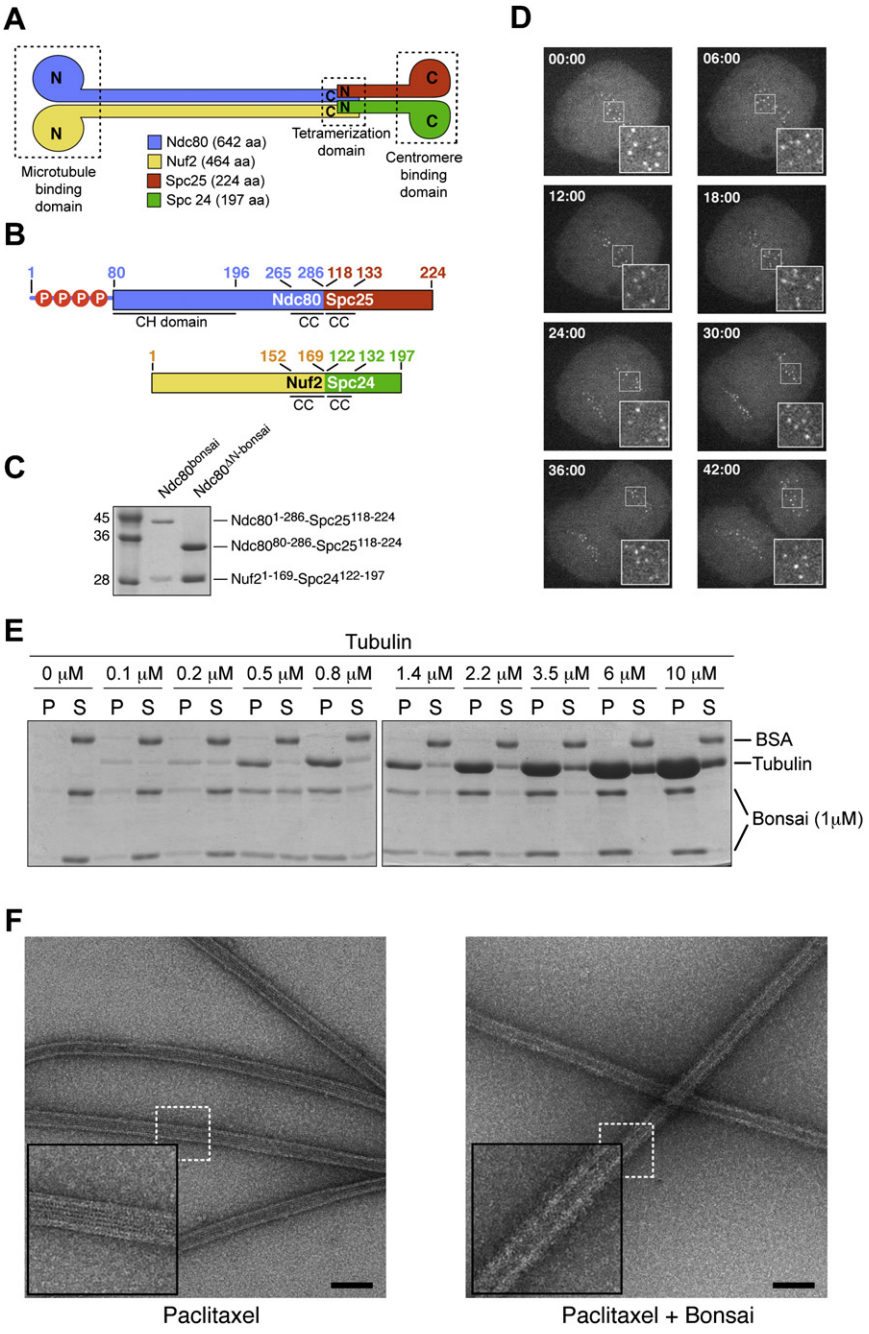

Figure 1. Properties of Ndc80^{bonsai}

(A) Organization of Ndc80 subunits.

(B) Scheme of Ndc80-Spc25 and Nuf2-Spc24 fusion proteins. Residues 1–286 of Ndc80 (Ndc80$^{1–286}$) were fused to residues 118–224 of Spc25 (Spc25$^{118–224}$). Residues 1–169 of Nuf2 (Nuf2$^{1–169}$) were fused to residues 122–197 of Spc24 (Spc24$^{122–197}$). Red circles with "P" mark phosphorylation sites in the Ndc80 N-terminal tail (Cheeseman et al., 2006; DeLuca et al., 2006; Wei et al., 2007).

(C) Ndc80-Spc25 and Nuf2-Spc24 fusions were coexpressed in *E. coli* and purified to homogeneity.

(D) When injected in HeLa cells, Alexa Fluor 488-labeled Ndc80^{bonsai} stained kinetochores throughout mitosis.

(E) Partition of the Ndc80^{bonsai} complex in pellet (P) and supernatant (S) fractions in cosedimentation assay with increasing concentrations of polymeric tubulin.

(F) Negative stain EM images of Paclitaxel-stabilized microtubules in the absence (left) and presence (right) of bound Ndc80^{bonsai}. A thick halo of protein surrounds the microtubules bound by Ndc80^{bonsai}, giving them a hairy appearance. Insets are 2.5×. Bar = 100 nm.

et al., 2005) revealed a long rod with globular domains at either end (Figure 1A). The globular regions of Nuf2 and Ndc80 occupy one end of the rod and are located near the N termini of these proteins (Ciferri et al., 2005; Wei et al., 2005). A heterodimeric coiled coil engaging Nuf2 and Ndc80 and emerging from the globular region accounts for most of the central shaft (Figures 1A and S1). The C-terminal end of the Nuf2-Ndc80 coiled coil encounters the N-terminal coiled coil of an Spc24-Spc25 subcomplex. The latter extends to the distal end of the rod, which contains a compact globular domain formed by the interacting heads of Spc24 and Spc25 (Ciferri et al., 2005; Wei et al., 2005, 2006). In vitro, Ndc80-Nuf2 and Spc24-Spc25 form stable subcomplexes that can self-assemble into the ~57 nm full-length Ndc80 complex (Ciferri et al., 2005; Wei et al., 2005).

Both globular regions of the Ndc80 complex are functionally important. The globular region of Spc24-Spc25 is important for kinetochore localization. It maps "internally" (i.e., closer to the centromere) relative to the Ndc80-Nuf2 globular head (Bharadwaj et al., 2004; Ciferri et al., 2005; DeLuca et al., 2006; Gillett et al., 2004). Conversely, the globular head of the Ndc80-Nuf2 moiety binds to microtubules (Cheeseman et al., 2006; Wei et al., 2007). The globular region of the Ndc80 subunit folds as a calponin-homology (CH) domain (Wei et al., 2007). CH domains in different proteins have been implicated in actin or microtubule binding (Gimona et al., 2002; Korenbaum and Rivero, 2002). The isolated CH domain of Ndc80 binds poorly to microtubules, suggesting that additional segments of the Ndc80 complex are required to create a functional microtubule-binding interface (Wei et al., 2007).

By combining protein engineering, X-ray crystallography, mass spectrometry, and biochemical methods, we characterized the architecture of the Ndc80 complex and the organization of the microtubule-binding interface of the Ndc80 complex.

Table 1. Data Collection, Phasing, and Refinement Statistics

Data Collection and Phasing	Native	Derivative
ESRF beamline	ID23-1	BM16
Space group	$P2_12_12$	$P2_12_12$
Unit cell parameters (Å,°)	a = 157.65, b = 248.97, c = 58.25, $\alpha = \beta = \gamma = 90$	a = 157.21, b = 250.15, c = 58.28, $\alpha = \beta = \gamma = 90$
Wavelength (Å)	0.954	0.979
Resolution limits (Å)[a]	50–2.88 (2.96–2.88)[a]	50–3.50 (3.63–3.50)[a]
Reflections: partials/full/unique	1,019,237/252,016/52,754	2,691,322/781,156/29,799
Completeness (%)	99.1 (99.8)[a]	99.7 (99.8)[a]
R_{sym}[b] (%)	9.9 (47.2)[a]	13.6 (64.9)[a]
I / σI	14.9 (4.2)[a]	25.9 (8.3)[a]
Redundancy	4.8 (4.7)[a]	26.2 (24.6)[a]
SAD Phasing		
SHELXD CC/CC (weak)		46.95/22.24
Se sites found/expected		33/36
FOM before solvent flattening and density modification (SHARP)		0.46
FOM after solvent flattening and density modification (Solomon/DM)		0.79
Refinement		
Resolution[c] (Å)	50–2.88 (2.96–2.88)[c]	
Reflections for R_{cryst} / for R_{free}	49,837/2,647	
R_{cryst}[d] (%)	23.2 (32.8)[c]	
R_{free}[d] (%)	26.1 (40.7)[c]	
No. of protein atoms/No. of solvent atoms	8,210/22	
Average B factor protein atoms (Å^2)	58.3	
Solvent content (%)	75	
Rmsd bond lengths (Å)	0.013	
Rmsd bond angles (°)	1.39	

FOM: figure of merit.
[a] Values in parentheses correspond to highest resolution shell.
[b] $R_{sym} = \Sigma_h\Sigma_i \mid I_{h,i} - < I_h > \mid / \Sigma_h\Sigma_i I_{h,i}$.
[c] Values in parentheses correspond to highest resolution shell used in refinement.
[d] R_{cryst} and $R_{free} = \Sigma \mid F_{obs} - F_{calc} \mid / \Sigma F_{obs}$; R_{free} calculated for a 5% subset of reflections not used in the refinement.

RESULTS

Generation of a Human "Bonsai" Ndc80 Complex

Reconstituted full-length human Ndc80 complex was refractory to crystallization and therefore to high-resolution structural analysis. To promote crystallization, we removed a large part of the coiled-coil region to generate a shorter and less flexible version of the complex. As the C-terminal regions of Nuf2 and Ndc80 contact the N-terminal regions of Spc24 and Spc25, we also reasoned that it should be possible to fuse these chains. We were successful in creating Ndc80-Spc25 and Nuf2-Spc24 chimeric chains containing short segments (15–60 residues) of the original coiled-coil sequences (Figure 1B). Coexpressed in bacteria, the fusion proteins gave rise to soluble and stable complexes, two of which will be discussed in detail: the $Ndc80^{1–286}$-$Spc25^{118–224}$:$Nuf2^{1–169}$-$Spc24^{122–197}$ complex, to which we refer as bonsai Ndc80 ($Ndc80^{bonsai}$); and the $Ndc80^{80–286}$-$Spc25^{118–224}$:$Nuf2^{1–169}$-$Spc24^{122–197}$ complex, to which we refer as $Ndc80^{\Delta N\text{-}bonsai}$, where ΔN stands for "*N*-terminal *d*eletion" (Figure 1C).

$Ndc80^{bonsai}$ Binds Kinetochores and Microtubules

We fluorescently labeled $Ndc80^{bonsai}$ with Alexa fluor 488 (Alexa-$Ndc80^{bonsai}$), injected it in early prometaphase HeLa cells, and followed its localization by live-cell video microscopy. Alexa-$Ndc80^{bonsai}$ localized to kinetochores throughout mitosis and until telophase (Figure 1D), similarly to the full-length counterpart (Bharadwaj et al., 2004; Ciferri et al., 2005; DeLuca et al., 2005, 2006; Hori et al., 2003; Liu et al., 2006; McCleland et al., 2004). We did not observe conspicuous perturbations of mitosis in the presence of $Ndc80^{bonsai}$.

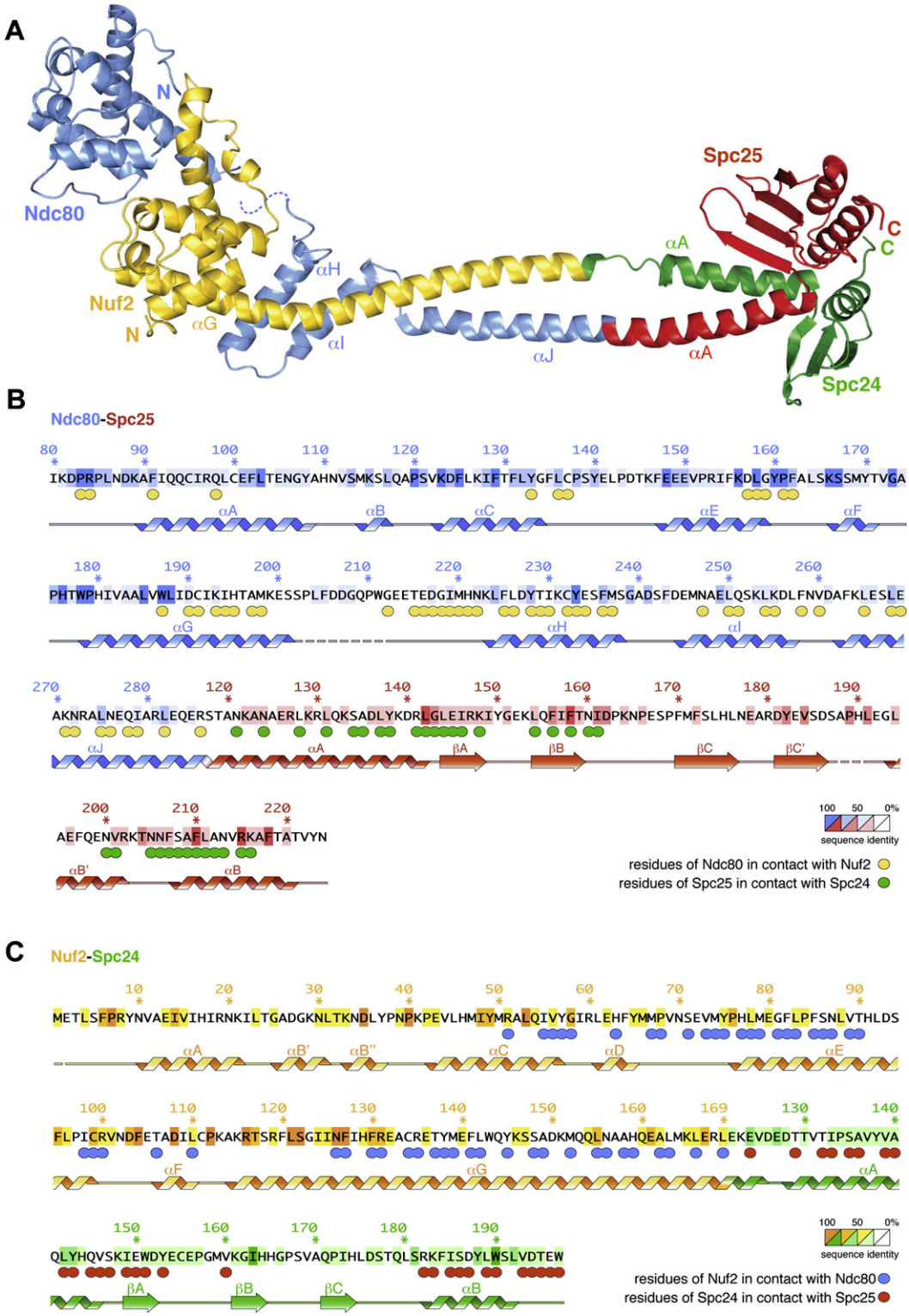

Figure 2. Crystal Structure of Ndc80$^{\Delta N\text{-bonsai}}$

(A) Ribbon model of Ndc80$^{\Delta N\text{-bonsai}}$. The structure is colored as in Figure 1A.

(B) Sequence of the Ndc80-Spc25 fusion protein. Numbering refers to human sequences. Residues are colored based on level of conservation. Circles under residues indicate a contact, and the color of the circle is the color of the contacted subunit (for instance, yellow = Nuf2). Residues are in contact when they

Cosedimentation of Ndc80^{bonsai} as a function of increasing microtubule concentrations (Figure 1E) revealed that Ndc80^{bonsai} binds tightly to microtubules (quantifications are presented in Figures 4 and S2 and Table S1). Microtubule binding by Ndc80^{bonsai} was also visually inspected using negative stain electron microscopy (EM). Paclitaxel- and GMPCPP-stabilized microtubules incubated with Ndc80^{bonsai} appeared "hairy," consistent with the idea that Ndc80^{bonsai} binds the microtubule lattice. In contrast, the surfaces of unbound microtubules appeared smooth (Figures 1F and S3). Although we were unable to visualize individual complexes, probably due to the relatively short dimensions of Ndc80^{bonsai}, these results recapitulate previous negative stain EM analyses obtained with a tetrameric full-length Ndc80 complex or with the Ndc80-Nuf2 subcomplex (Cheeseman et al., 2006; Wei et al., 2007).

In summary, Ndc80^{bonsai} retains the ability to bind microtubules and to localize to kinetochores, two fundamental biological properties of the full-length Ndc80 complex.

Crystal Structure of Ndc80$^{\Delta N\text{-}bonsai}$

We crystallized Ndc80$^{\Delta N\text{-}bonsai}$ and determined its crystal structure to 2.9 Å resolution with phases from a single-wavelength anomalous dispersion (SAD) experiment (Table 1 and Experimental Procedures). So far, we have been unable to crystallize Ndc80^{bonsai}, possibly because the N-terminal tail of Ndc80 (residues 1–79) is disordered.

With a long axis of ~150 Å, Ndc80$^{\Delta N\text{-}bonsai}$ is much shorter than the 570 Å full-length Ndc80 complex (Ciferri et al., 2005; Wei et al., 2005). At one end of the rod, a globular helical domain of Nuf2 (residues 1–130) is sandwiched between the CH domain (residues 87–201) (Wei et al., 2007) and a helical hairpin (helices αH-αI, residues 221–258) of Ndc80 (Figure 2A). The Ndc80 CH domain and helical hairpin are connected through a disordered segment (residues 202–215). From residues 265^{Ndc80} and 152^{Nuf2}, the polypeptide chains of Ndc80 and Nuf2 form a coiled coil that merges directly into the Spc24-Spc25 moiety (Figures 2A–2C). The ~70 Å coiled-coil region is only briefly interrupted near the beginning of Spc24, possibly as an artifact of the fusion design. The globular regions of Spc24 and Spc25 mark the opposite end of the molecule relative to Ndc80-Nuf2. They are structurally related, and their fold consists of a three- or four-stranded β sheet, which packs against one or two α helices (Figures 2A–2C and S4), as shown previously for the homologous subunits of *Saccharomyces cerevisiae* (Wei et al., 2006). Spc24 and Spc25 associate tightly in a single globular entity through a conserved interface (Figure S4), while a few conserved exposed residues define a putative site of interaction with unknown kinetochore partners (Wei et al., 2006).

A CH Domain in Nuf2

The globular region of Ndc80 folds as a CH domain (Wei et al., 2007). The structure of Ndc80$^{\Delta N\text{-}bonsai}$ reveals that residues 1–130 of Nuf2 also fold as a CH domain (Figure 3). CH domains appear in proteins of different functions (Castresana and Saraste, 1995; de Arruda et al., 1990). They belong to different sequence classes and are usually present in one, two, or four copies (Gimona et al., 2002; Korenbaum and Rivero, 2002). The core of the CH domain is a four-helix bundle containing the parallel helices αA, αC, αE, and αG. These are connected by long external loops often but not always containing three additional short and irregular helices (αB, αD, αF). For instance, αD is absent in the Ndc80 CH domain but is present in the Nuf2 CH domain (Figure 3A).

The Nuf2 CH domain is irregular. Its αE helix bends at both ends due to the presence of proline and glycine residues (Figures 2 and 3). The first half of αE protrudes away from the core of the four-helix bundle to provide an interaction surface for the Ndc80 CH domain (see below). The αE helix orients at an almost right angle relative to the αC-αG pair. This orientation is stabilized by the αF helix, which packs against the αC-αG thanks to a conserved and partially buried salt bridge between Asp108^{Nuf2} and Arg116^{Nuf2}. At the C-terminal end, the αG helix of Nuf2 extends away from the Nuf2 CH globular domain, interacting first with the αH-αI hairpin of Ndc80 and then merging directly into the coiled coil where it pairs with the αJ helix of Ndc80 (Figure 2A).

Structure-based superposition of the Ndc80 and Nuf2 CH domains yields a root-mean-square deviation (rmsd) of 2.4 Å over ~90 C_α atoms (Figure 3B). An equivalent superposition with the CH domain of EB1 (Hayashi and Ikura, 2003; Slep and Vale, 2007) yields an rmsd of 3.5 Å over 79 C_α atoms (Figure S5). A sequence alignment based on structural alignment of the CH domains of Nuf2, Ndc80, and EB1 shows that the CH domains of Nuf2 and Ndc80 have only ~6% sequence identity and that the conservation is located predominantly in the hydrophobic core (Figure 3C). The aligned surfaces lack conspicuous conserved features. The Nuf2 CH domain also has negligible sequence similarity to other CH domains.

The compact assembly of the Ndc80 and Nuf2 CH domains is capped by the αH-αI hairpin of Ndc80. The assembly has approximate dimensions of 75 Å × 35 Å × 35 Å and is maintained by an interface burying ~2300 Å^2 on each participant and distributed over two major areas (Figure 3D). The first area involves the αD-αE loop and the αE and αF helices of Nuf2 and the ~20 residue insertion between them. These pack against the αE-αF loop and the αG helix of Ndc80. This region contains Trp187^{Ndc80}, which is very well conserved. It donates a hydrogen bond to the main chain carbonyl of Leu78^{Nuf2}, situated in the irregular segment at the beginning of αE^{Nuf2}. The second area involves the C-terminal ends of the αC and αE helices and the extension of the αG helix of Nuf2 (after residue 126). These pack against the αH-αI helical hairpin of Ndc80. The interface between the CH domains of Nuf2 and Ndc80 is predominantly hydrophobic, suggesting that the two domains interact stably.

Tandem CH domains have been implicated as actin-binding modules in proteins such as α-actinin, filamin, and β-spectrin (Gimona et al., 2002; Korenbaum and Rivero, 2002). In these proteins, the tandem CH domains have a similar pseudo 2-fold orientation characterized by the packing of the αA and

form hydrogen bonds or salt bridges, or when they are less than 4 Å away, or when they bury more than 40% of the solvent-accessible surface in the interaction, calculated with PISA (Krissinel and Henrick, 2007).

(C) Sequence of the Nuf2-Spc24 fusion analyzed as in (B).

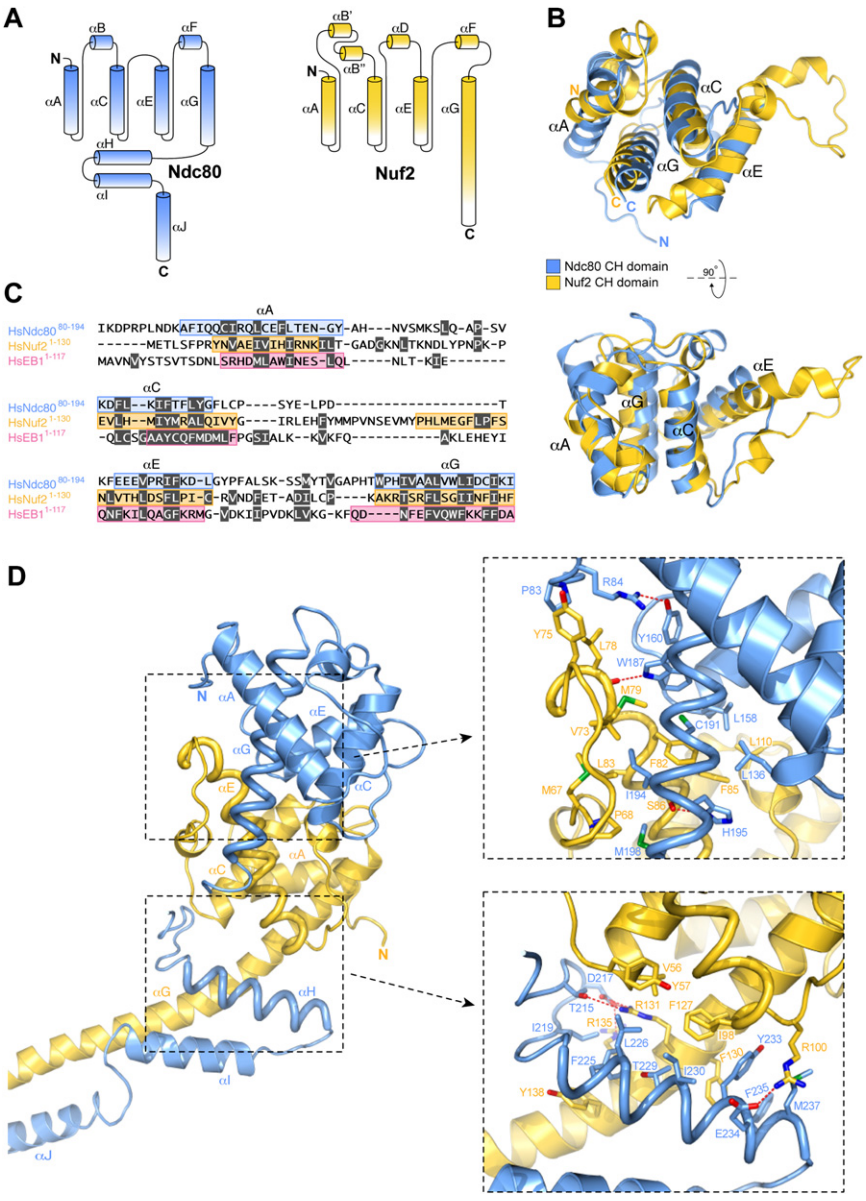

Figure 3. Organization of the CH Domains in the Ndc80-Nuf2 Subcomplex

(A) Topology diagram of Ndc80 and Nuf2. The CH domain is contained between the αA and αG helices.

(B) Two views of the superposition of the CH domains of Ndc80 and Nuf2. Note the conspicuous bending of the tips of the Nuf2 αE helix.

(C) Structure-based sequence alignment of the CH domains of Ndc80, Nuf2, and EB1. The αA, αC, αE, and αG helices are contoured. Residues highlighted in gray have their side chains buried in the hydrophobic core of the CH domain.

(D) General view and closeups of the interface of Ndc80 and Nuf2.

the αG helices of the first CH domain against the αA and the αG helices of the second domain (Figure S5). The interaction between the Ndc80 and Nuf2 CH domains follows a clearly distinct pattern. The two CH domains are rotated so that the αA helices are at the periphery of the dimeric assembly, rather than at its interface (Figure S5). Thus, pairs of CH domains interacting intra- or intermolecularly do not have an obligate reciprocal orientation.

The Microtubule-Binding Interface

We analyzed residue conservations and charge distributions of the continuous surface of the Ndc80-Nuf2 globular region (Figure 4). Most conserved surface-exposed residues (identified based on the alignment in Figure S6) map to the face of the Ndc80-Nuf2 globular head that points away from the direction of the coiled coil (Figure 4A, left). Most residues on this face are located in the αC, αE, and αF helices and in the αE-αF loop of Ndc80, and in the αB-αC and αF-αG loops and in the αF helix of Nuf2. The opposite face of the Ndc80-Nuf2 globular region fails to reveal significant conservation (Figure 4A, right).

The CH domains of Ndc80 and Nuf2 have predicted isoelectric points (pI) of 7.4 and 8.0, respectively. Two positively charged patches, separated by a negatively charged ridge, characterize the surface of the Ndc80-Nuf2 globular head (Figure 4B, left panel). This tripartite charge distribution is largely conserved from yeast to man, as revealed by modeling of the sequences of Ndc80 and Nuf2 from several species onto the crystal structure of $Ndc80^{\Delta N\text{-}bonsai}$ (Figure S7). In the human Ndc80 and Nuf2 structures, the positive patches include $Lys89^{Ndc80}$, $Lys115^{Ndc80}$, $Lys123^{Ndc80}$, $Lys146^{Ndc80}$, $Lys156^{Ndc80}$, $Lys166^{Ndc80}$, $Lys29^{Nuf2}$, $Lys33^{Nuf2}$, $Lys41^{Nuf2}$, and $Lys115^{Nuf2}$ (Figure 4C), none of which is fully conserved (Figure S6). To test the contribution of these residues toward microtubule binding, we mutated them into alanine (KA) or glutamic acid (KE) in the framework of $Ndc80^{bonsai}$. Additionally, we generated combinations of KA mutants (Table S1). After purification to homogeneity, we tested the ability of the resulting mutants to cosediment with microtubules.

Wild-type $Ndc80^{bonsai}$ bound microtubules with an apparent dissociation constant (K_D) of ~40 nM (Figure 4D, Supplemental Experimental Procedures, and Table S1). Strong impairment of microtubule binding (30- to 40-fold reduction of apparent K_D) was observed with KE mutants of $Lys89^{Ndc80}$, $Lys166^{Ndc80}$, and $Lys115^{Nuf2}$ (Figure 4D, left panel and Table S1). The equivalent KA mutants gave a >6-fold impairment of microtubule binding (Figure 4D, central panel). A 6- to 12-fold reduction of apparent K_D was also observed with KE mutants of $Lys146^{Ndc80}$, $Lys156^{Ndc80}$, $Lys33^{Nuf2}$, and $Lys41^{Nuf2}$ (Table S1). Although some of the equivalent KA mutants had only a modest effect

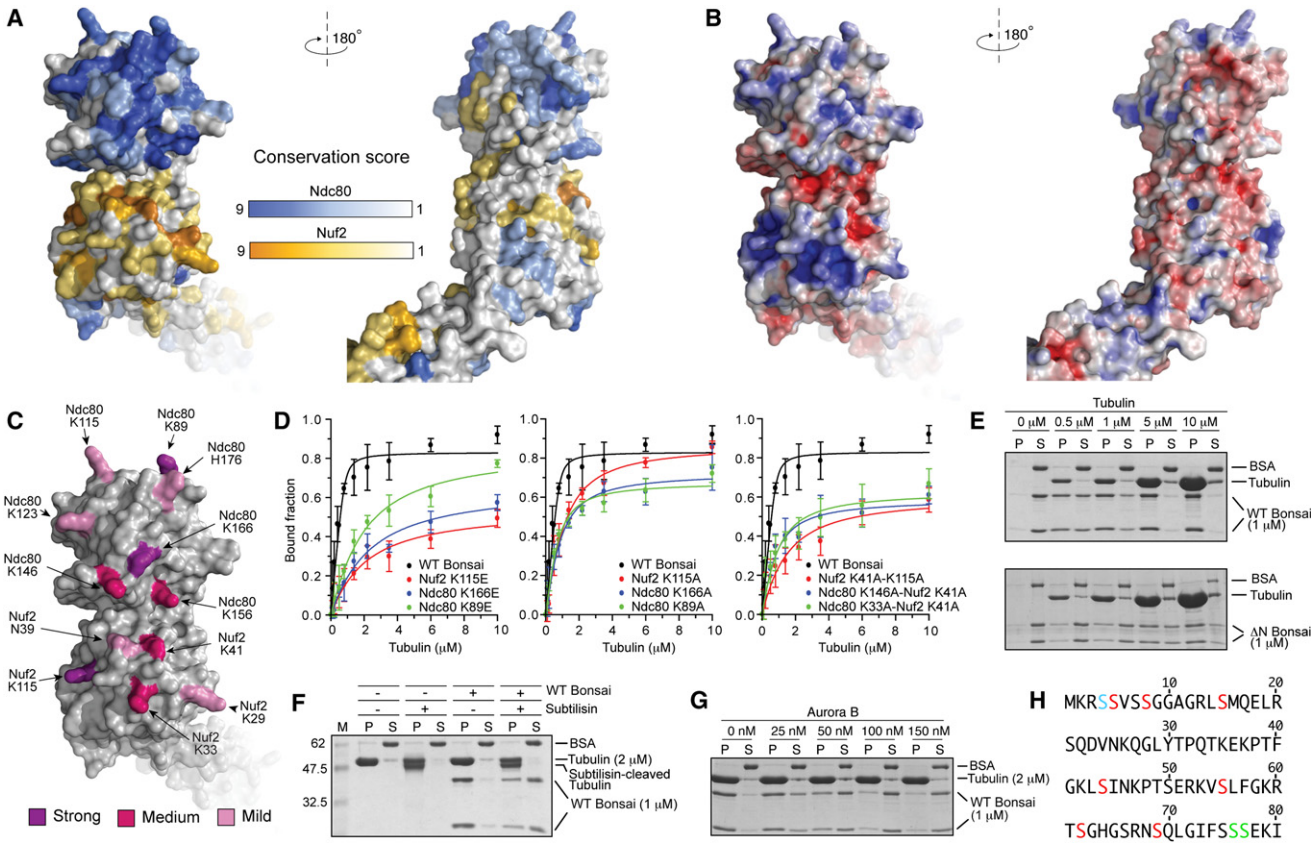

Figure 4. Organization of the Microtubule-Binding Region

(A) Surface views of the Ndc80-Nuf2 globular region colored according to conservation.

(B) Surface views colored by electrostatic potential. The orientations are as in (A).

(C) Positions of mutated residues. Residues whose KE mutation caused a 30- to 40-fold impairment of microtubule binding are shown in purple (see also panel D, Table S1, and Figure S2). Residues whose KE mutation caused a 6- to 12-fold impairment in microtubule binding are shown in magenta. Residues whose mutation into alanine provided modest destabilization of binding that was not quantitated are shown in pink.

(D) Plot of quantifications of microtubule cosedimentation assay with Ndc80^{bonsai} and the indicated mutants (see also Table S1 and Figure S2). Error bars represent standard deviations calculated from at least three independent experiments.

(E) The ability of Ndc80^{bonsai} and Ndc80$^{\Delta N\text{-}bonsai}$ to cosediment with microtubules was tested in parallel.

(F) Ndc80^{bonsai} showed strongly reduced binding to subtilisin-treated microtubules (see Supplemental Experimental Procedures for details).

(G) Aurora B releases Ndc80^{bonsai} from microtubules.

(H) Sequence of the N-terminal tail of Ndc80. Residues in red were phosphorylated by Aurora B in vitro (see Supplemental Experimental Procedures). Residues in green are phosphorylated in vivo but do not conform to the Aurora B consensus. Ser4 (blue) could not be assigned unambiguously.

on microtubule binding, their combination with other mutants gave clear additive effects (Figure 4D, right panel and Table S1). Moderate negative effects on microtubule binding were also observed with alanine mutants of Lys115^{Ndc80}, Lys123^{Ndc80}, His176^{Ndc80}, Lys29^{Nuf2}, and Asn39^{Nuf2}, but the effects of these mutants on microtubule binding were not quantitated.

The N-terminal region of the Ndc80 subunit has an estimated pI of about 11. Compared to Ndc80^{bonsai}, Ndc80$^{\Delta N\text{-}bonsai}$ is an ~100-fold weaker microtubule binder (with an approximate K_D of 4–5 μM as inferred from Figure 4E), in agreement with previous results (Wei et al., 2007). The acidic C-terminal tails of α- and β-tubulin are implicated in the binding of microtubule-binding proteins (Cassimeris and Spittle, 2001). To test the role of the acidic C-terminal tails of tubulin in Ndc80^{bonsai} binding, we proteolytically removed them using the protease subtilisin. Microtubules assembled from tubulin lacking the acidic C-terminal tails showed dramatically reduced binding to Ndc80^{bonsai} (Figure 4F).

In summary, our results indicate that (1) both Ndc80 and Nuf2 are required for microtubule binding; (2) a large fraction of the continuous conserved surface shown in Figure 4A is implicated in microtubule binding; (3) the N-terminal region of Ndc80 contributes to microtubule binding; (4) the microtubule-binding interface of the Ndc80 complex contains several positively charged residues; and (5) the acidic C-terminal tails of tubulin are required for the interaction of Ndc80 with microtubules. We conclude that the interaction of the Ndc80 complex with microtubules is eminently based on electrostatic interactions.

Ndc80^{bonsai} detached from microtubules in the presence of active Aurora B kinase (Sessa et al., 2005) and ATP (Figure 4G).

Using mass spectrometry, we determined that Aurora B phosphorylates Ndc80 at Ser5, Ser8, Ser15, Ser44, Ser55, Ser62, and Ser69 (Figure 4H). Ser4 was also potentially phosphorylated, but it could not be assigned unambiguously. With the exception of Thr49, whose phosphorylation we could not confirm, our sites confirm and extend the list of in vitro (Ser5, Ser15, Thr49, Ser55, and Ser69) or in vivo (Ser55 and Ser62) Aurora B sites identified previously (DeLuca et al., 2006; Nousiainen et al., 2006). Two additional in vivo phosphorylation sites, Ser76 and Ser77 (Nousiainen et al., 2006), do not conform to the Aurora B consensus and were not identified in our experiments. In *C. elegans*, the four sites Thr8, Ser18, Ser44, and Ser51 of NDC80, which correspond to Ser8, Ser15, Ser44, and Ser55 of the human sequence, are Aurora B targets (Cheeseman et al., 2006). Thus, regulation of Ndc80-microtubule binding by Aurora B phosphorylation is a conserved theme in evolution (Cheeseman et al., 2006; DeLuca et al., 2006; Wei et al., 2007).

Evidence of Cooperativity in the Interaction of Ndc80 with Microtubules

We used fluorescence microscopy to examine the interaction of Ndc80^{bonsai} with microtubules. Rhodamine-labeled microtubules were mixed with different concentrations of Alexa-Ndc80^{bonsai} complex, and after 30 min the mix was transferred onto a coverslip and imaged by wide-field fluorescence microscopy. At low stoichiometry ratios of Ndc80^{bonsai} complex to polymeric tubulin (abbreviated as N/T ratio), fluorescence from the Ndc80^{bonsai} complex looked "patchy" (Figure 5). Line scans along the microtubules confirmed the presence of areas of high fluorescence intensity, interspersed with areas of background-level intensity. We show in the Supplemental Discussion that the high contrast of these images does not reflect the formation of fluorescent speckles, which are caused by a random distribution of fluorophores (Waterman-Storer and Salmon, 1998), but rather the clustering of Ndc80^{bonsai} complexes on microtubules. At higher N/T ratios, the fluorescence intensity from the Ndc80^{bonsai} complex became evenly distributed and its ratio to rhodamine-labeled tubulin became essentially constant all along the microtubule. The intensity of Ndc80^{bonsai} fluorescence to microtubule fluorescence became stable when the N/T ratio reached 1/1. The intensity of Ndc80^{bonsai} fluorescence to microtubule fluorescence in the clusters at substoichiometric N/T ratios was only ~2-fold lower than at saturating concentrations, suggesting that the density of Ndc80^{bonsai} complex within the clusters is almost saturating.

In summary, the binding of Ndc80^{bonsai} to microtubules might be cooperative—as suggested for the full-length complex (Cheeseman et al., 2006)—with initial seeds driving the growth of larger areas of bound Ndc80 molecules along the microtubule cylinder. As clustering is only observed at substoichiometric N/T ratios, we speculate that growth of clusters is limited by availability of Ndc80 subunits.

The structural bases for clustering of the Ndc80^{bonsai} complex on microtubules are unknown, but we suspect that the N-terminal tail of the Ndc80 subunit is involved. A fluorescent version of Ndc80$^{\Delta N\text{-}bonsai}$, which binds microtubules poorly in sedimentation assays (see above and Wei et al., 2007), stains microtubules evenly at substoichiometric N/T ratios and does not form clusters (data not shown). Due to the reduced microtubule-binding affinity of Ndc80$^{\Delta N\text{-}bonsai}$, however, the fluorescence intensity is rather dim and unsuitable to support our case incontrovertibly. As Ndc80^{bonsai} is monodisperse, its binding to microtubules in clusters at substoichiometric N/T ratios is unlikely to reflect aggregation, but it remains possible that clustering results from an artifactual intermolecular interaction caused by chain truncation or chain fusion in the engineered Ndc80 complex. We asked if Ndc80$^{\Delta N\text{-}bonsai}$ could form patches in the presence of a stoichiometric amount of unlabeled Ndc80^{bonsai}. The presence of unlabeled Ndc80^{bonsai} failed to promote the incorporation of Ndc80$^{\Delta N\text{-}bonsai}$ in patches on the microtubule (data not shown). This argues against an artifactual aggregation phenomenon and suggests that the N-terminal tail is required in *cis* to promote clusters on microtubules.

DISCUSSION

The ability of the Ndc80 complex to bind microtubules is based on a pair of tightly packed CH domains in the Ndc80 and Nuf2 subunits. CH domains are present in other microtubule-binding proteins, including CLAMP (Dougherty et al., 2005) and EB1 family members, which form dimers. The structure of the isolated CH domain of EB1 is known (Hayashi and Ikura, 2003; Slep and Vale, 2007), but it is unknown how the CH domains are organized in the EB1 dimer. The available data suggest that the microtubule-binding interface on the EB1 CH domain (Hayashi and Ikura, 2003; Slep and Vale, 2007) is different from each of the two distinct microtubule-binding interfaces identified in the CH domains of Ndc80 and Nuf2. Thus, there is considerable plasticity in the mechanisms whereby CH domains recognize microtubules. It was reported recently that EB1 binds to the microtubule seam (Sandblad et al., 2006). Our low-resolution binding studies with stabilized microtubules, and previous analogous studies (Cheeseman et al., 2006; Wei et al., 2007), show that Ndc80 decorates the entire microtubule lattice. In the future, it will be important to study the binding of Ndc80 to dynamic microtubules and to assess whether EB1 and the Ndc80 complex can coexist on the same microtubule lattice, i.e., whether or not they compete for the same binding sites on microtubules.

Two positively charged patches are the most prominent surface features contributed by the Ndc80 and Nuf2 CH domains. The distance between the center of mass of the two CH domains (~30 Å) is similar to the distance between the beginnings of the acidic C-terminal tails in a tubulin dimer (~32 Å). This supports the speculation that each CH domain binds one of the two acidic tails in a tubulin dimer (Figure 6A). In preliminary experiments, we failed to detect significant binding of Ndc80^{bonsai} to soluble tubulin dimers (data not shown), suggesting that additional interactions on the microtubule lattice increase the binding affinity. The N-terminal tail of Ndc80, a low-complexity sequence that is unlikely to adopt a stable folded conformation on its own (Figure 4H), is essential for tight microtubule binding. It might contribute directly to microtubule binding, possibly allowing the alignment of the Ndc80 CH domain toward the minus end and of the Nuf2 CH domain toward the plus end (Figures 6A and 6B). Our results suggest that the binding of Ndc80 to microtubules is cooperative (Figure 5). We

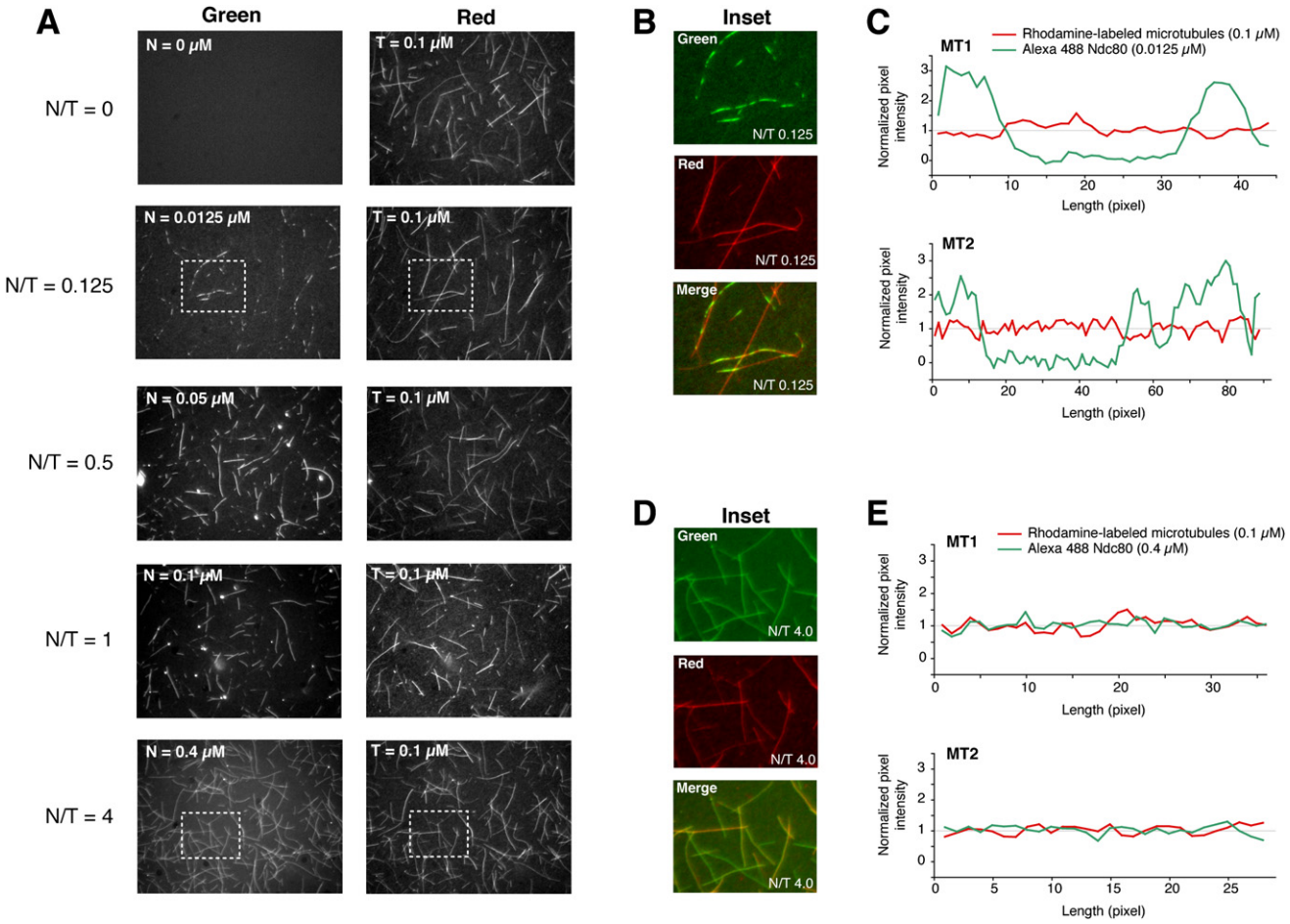

Figure 5. Visualization of Microtubule Binding

(A) A mix of rhodamine-labeled tubulin:tubulin at a 0.16 ratio and final concentration of 100 nM was polymerized and incubated with increasing amounts of Alexa-Ndc80^{bonsai}. N/T is the Ndc80^{bonsai}/tubulin concentration ratio.

(B) Inset from N/T = 0.125 showing clusters of fluorescent Ndc80^{bonsai} on microtubules.

(C) Line scans of two representative microtubules. The net fluorescence intensity (signal − background) at each pixel was divided by the mean net fluorescence intensity along the line scan.

(D) Inset from N/T = 4.0 showing even distribution of Ndc80^{bonsai}.

(E) Line scans of two representative microtubule analyses as for (C).

thought of two models by which this could be achieved. In Figure 6B, cooperativity is achieved by a ''lateral'' interaction of the Ndc80 complexes, which becomes available only in the presence of a prebound complex. As the dimensions of the microtubule-binding surface of the Ndc80 complex (55 Å × 35 Å) are significantly smaller than those of the tubulin dimer (85 Å × 45 Å on the exposed surface), it is difficult to envision how neighboring Ndc80 complexes would form extensive intermolecular contacts when bound to the microtubule lattice. In Figure 6C, cooperativity is achieved through the N-terminal tail, which is postulated to bind to an acidic patch of a neighboring Ndc80 complex rather than to microtubules.

While ensuring sturdy connections, the microtubule-binding interface must remain dynamic to allow rapid sliding along a polymerizing or depolymerizing microtubule. Increased stability of the microtubule-kinetochore connections leads to excessive centromeric tension and interference with chromosome segregation (Cimini et al., 2006; DeLuca et al., 2006). Phosphorylation of the N-terminal tail of Ndc80 by Aurora B, which destabilizes the interaction with microtubules (Figure 4 and Cheeseman et al., 2006; DeLuca et al., 2006), is required to maintain a dynamic Ndc80-microtubule connection. The consensus site of the Aurora B kinase ([R/K]-[R/K]-X-[S,T]) is ideally suited to regulate microtubule-binding proteins because the positive charges in this motif have the potential to mediate the binding to the negatively charged microtubules but can be rapidly neutralized by phosphorylation. Alternatively, it is possible that the phosphorylated N-terminal tail of Ndc80 competes, through an intramolecular interaction, with the acidic C-terminal tails of tubulin for the positively charged sites within the tandem CH homology domain (Figure 6D). In either case, the phosphorylation of multiple target sequences in the N terminus of Ndc80

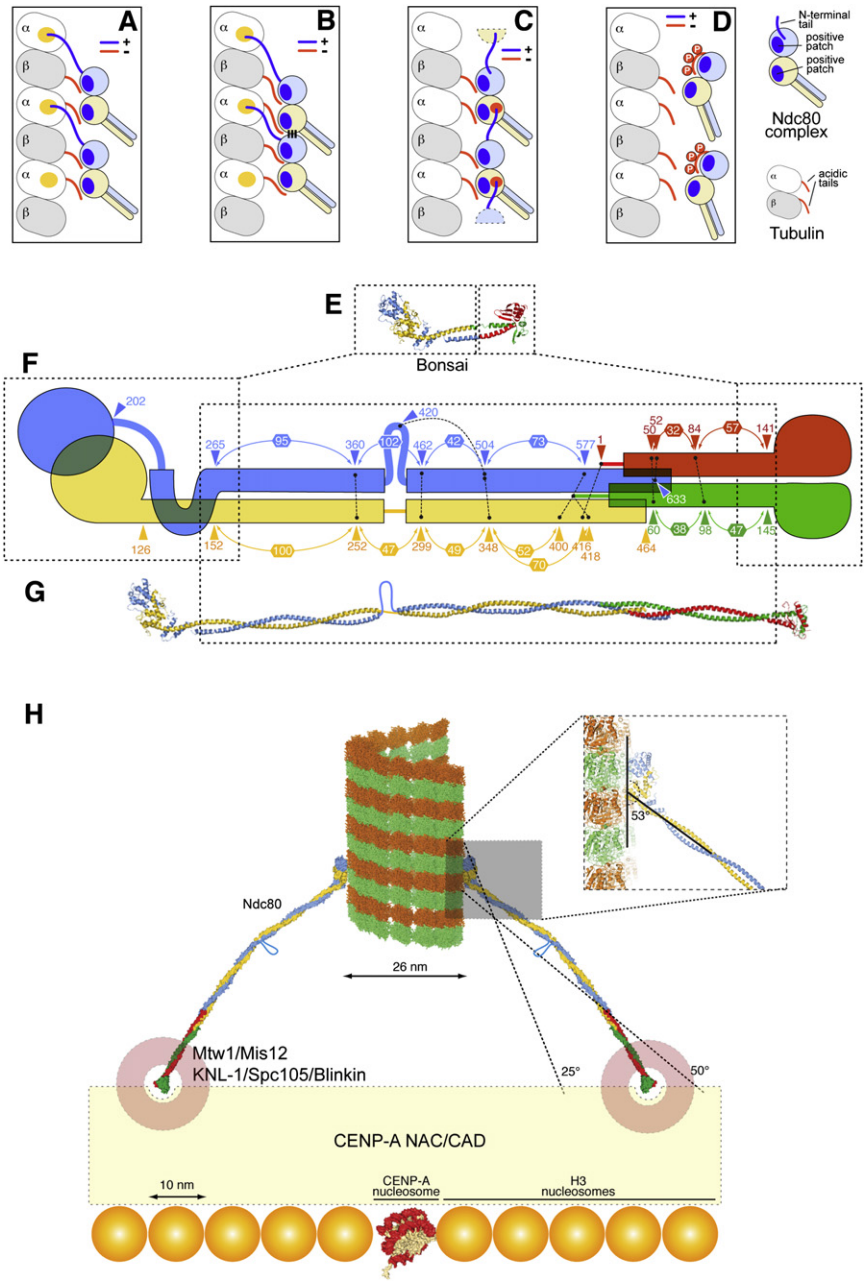

Figure 6. Models of Ndc80 and Microtubule-Kinetochore Interaction

(A–D) Models of the Ndc80-microtubule interaction. A yellow patch on tubulin in (A) and (B) represents a hypothetical binding site for the Ndc80 N-terminal tail. In (C), it is hypothesized that the N-terminal tail binds to the negatively charged patch on Nuf2, shown in Figure 4B.

(E) The Ndc80^{bonsai} complex.

(F) Summary of crosslinking analysis (Maiolica et al., 2007). Connected black dots mark crosslinked residues. Numbers in hexagons define distances between "milestones," such as subsequent crosslinked residues or pairs of interacting residues identified in the structure.

(G) Model of the full-length Ndc80 complex showing the predicted break in the coiled-coil region.

(H) Implications from the structure of the Ndc80 complex on the organization of the microtubule-kinetochore interface.

might represent an additional example of ultrasensitivity in a protein-protein interaction (Serber and Ferrell, 2007).

Cells injected with the 9G3 monoclonal antibody show hyperstabilized kinetochore-microtubule connections (DeLuca et al., 2006). 9G3 binds to residues 200–215 of human Ndc80, located in a disordered loop connecting the CH domain to the αH-αI hairpin. In vitro, 9G3 partially impairs the ability of Aurora B to phosphorylate the Ndc80 N-terminal region (DeLuca et al., 2006). Although the N-terminal 79 residues are missing from our structure, we note that the epitope recognized by 9G3 is ~30 Å away from residue 80^{Ndc80} (the first visible residue in the structure of Ndc80$^{\Delta N\text{-bonsai}}$). A bulky antibody structure might be expected to at least partially impair the access of the N-terminal tail to the active site of Aurora B kinase. Our results in Figure 5 suggesting that the Ndc80 complexes cluster on microtubules are also consistent with an alternative explanation: the bivalent (IgG) 9G3 antibody might crosslink neighboring Ndc80 complexes, effectively coupling their microtubule-binding sites and increasing their apparent affinity for microtubules. Our preliminary results (not shown) are consistent with this possibility.

To advance our comprehension of the overall organization of the Ndc80 complex, we subjected a recombinant version of the quaternary, full-length Ndc80 complex (Ciferri et al., 2005) to a crosslinking and mass spectrometry analysis, a technical description of which has been published separately (Maiolica et al., 2007). We identified 26 sites in which the subunits of the Ndc80 complex were crosslinked, either intra- or intermolecularly, by BS^{2}G, a 7.7 Å bifunctional molecule targeting the primary amino group of lysine or of the N-terminal residue (Maiolica et al., 2007). The crosslinks provide information on the register of the coiled-coil regions in the central shaft of the Ndc80 rod and on the mechanism of chain overlap in the tetramerization domain (Figure 6F and Supplemental Discussion).

With the register of the coiled coils in hand, we produced a full-length model of the Ndc80 complex (Figure 6G). The only conspicuous deviation from the coiled-coil organization of the shaft is an ~50 residue insertion in Ndc80, in correspondence to a region showing decreased coiled-coil propensity (residues 420–460 of Ndc80, Figure S1). Based on sequence conservation

and coiled-coil predictions, we suspect that the insertion in Ndc80 is conserved from yeast to man. The insertion might introduce flexibility to allow microtubule capture at different angles. Additional flexibility along the rod is also revealed by the analysis of the two Ndc80$^{\Delta N\text{-bonsai}}$ complexes in the crystal's asymmetric unit (Figure S8).

Low-resolution EM analyses revealed that the Ndc80 rods coat the microtubules at a 25° to 55° angle (Cheeseman et al., 2006). In Ndc80^{bonsai}, the coiled coil emerges from the globular domain with an angle of 53°–58° (Figure 6H; the two values refer to the two dimers in the crystal's asymmetric unit). It is possible that the slightly lower values observed by EM can be explained with flexibility in the Ndc80 subunit caused by the insertion in Ndc80 (see also legend to Figure 6H). The diameter of a microtubule is 26 nm. The distal ends of two 57 nm Ndc80 rods binding oppositely on the microtubule lattice (i.e., 180° away from each other) at angles comprised between 25° and 50° would be 75 to 110 nm apart.

At present, we do not know the exact identity of the kinetochore receptor of the Ndc80 complex. The Ndc80 complex binds to several additional kinetochore proteins and protein complexes, including KNL1/Spc105/Blinkin and Zwint-1, the Mtw1/Mis12 complex (also known as MIND complex), and the Ctf19 complex, also known as the COMA complex (Cheeseman and Desai, 2008). These proteins (with the possible exception of Zwint-1) are conserved in eukaryotes. At one end of the elongated Ndc80 complex, the Spc24-Spc25 globular dimeric head might tether to a "kinetochore receptor" formed by the KNL1-Mis12 complex, generating the so-called KMN network (for *K*NL1, Mtw1/*M*is12 complex, and *N*dc80, Cheeseman et al., 2006). In turn, these proteins are likely to interact with a network of inner kinetochore components, known as CENP-A NAC/CAD, that are believed to anchor to a centromere-specific CENP-A-containing nucleosome (Foltz et al., 2006; Okada et al., 2006). As the long axis of a nucleosome is 10 nm, the surface covered by the Ndc80 rods at a microtubule-binding site might extend over an area containing 7 by 7 up to 11 by 11 or more nucleosomes (Figure 6H). The point centromeres of *S. cerevisiae* are based on a 150 bp DNA sequence embedded in a specialized nucleosome containing the histone H3 variant CENP-A (named Cse4 in *S. cerevisiae*, see Cleveland et al., 2003; Maiato et al., 2004). The distribution of the centromere-specific Cse4-containing nucleosome has been debated, but recent studies support the idea that Cse4 marks a single nucleosome at the centomere (Furuyama and Biggins, 2007). It follows that the Ndc80 complexes that attach to the single microtubule at yeast kinetochores are unlikely to be located on the Cse4-containing nucleosome. We speculate therefore that H3-containing nucleosomes neighboring the Cse4-containing nucleosome might be endowed with the ability to recruit kinetochore components, including the Ndc80 complex. Future structural analyses will have to shed light on the organization of the KMN network and its interactions with the rest of the kinetochore.

EXPERIMENTAL PROCEDURES

Protein Expression and Purification

Full-length (fl) cDNAs encoding HsNuf2 and HsSpc24 were sequentially subcloned in pGEX6P-2rbs, a dicistronic derivative of pGEX-6P (GE Healthcare). cDNAs encoding HsNdc80 and HsSpc25 genes were also subcloned in pGEX6P-2rbs. To create the Nuf2-Spc24 chimera, Nuf2 and Spc24 cDNAs in pGEX6P-2rbs were fused by inverse PCR with oligonucleotides Nuf2(169Rev) and Spc24(122For) (Supplemental Experimental Procedures). To generate the Ndc80-Spc25 chimera, Ndc80 and Spc25 were fused with oligonucleotides Hec1(286Rev) and Spc25(118For). cDNAs encoding Nuf2-Spc24 and Ndc80-Spc25 were sequentially subcloned in pGEX6P-2rbs. Ndc80$^{\Delta N\text{-bonsai}}$ was created by PCR on the Ndc80-Spc25 chimera. This was used to replace the Ndc80-Spc25 chimera in the second cassette of pGEX6P-2rbs. Point mutants were created with QuikChange (Stratagene).

Ndc80^{bonsai} expression in *E. coli* BL21(DE3) was induced with 400 μM IPTG at OD_{600} = 0.45–0.6 for 12–16 hr at 20°C –25°C. Cells were harvested by centrifugation at 3500 *g*. Bacterial pellets were resuspended in lysis buffer (50 mM Tris-HCl, pH 7.6, 300 mM NaCl, 1 mM DTT, 1 mM EDTA, Complete Protease Inhibitor Cocktail Tablets [Roche]). Sonicated lysates were cleared by centrifugation at 40,000 rpm for 45–60 min on a Beckman 55.1 Ti rotor. Supernatants were incubated with 1 ml of GST Sepharose Fast Flow (GE Healthcare) per liter of bacterial culture. Beads were prewashed with PBS and equilibrated with lysis buffer. After 2–3 hr at 4°C, beads were washed with 30 volumes of lysis buffer and equilibrated in cleavage buffer (50 mM Tris-HCl, pH 7.6, 150 mM NaCl, 1 mM DTT, 1 mM EDTA). To cleave off GST, 10 units of PreScission protease (GE Healthcare) were incubated for 16 hr at 4°C per mg of substrate. The product in the flowthrough was concentrated up to 5 mg/ml by ultrafiltration in Vivaspin devices (Sartorius Stedim biotech, molecular weight cut-off 30,000) and loaded onto a Superdex 200 size exclusion chromatography (SEC) column (GE Healthcare) equilibrated with 25 mM Tris-HCl, pH 7.6, 150 mM NaCl, 1 mM EDTA, 1 mM dithiothreitol, 5% glycerol. Fractions containing the Ndc80 complex were collected and concentrated. Typically, 1–5 mg of pure complex was obtained per liter of bacterial culture. Mutant complexes were expressed and purified in essentially the same manner.

Crystallization and Structure Determination

Crystals were obtained with a point mutant of Ndc80$^{\Delta N\text{-bonsai}}$ in which Glu72 of Nuf2 is substituted with Gly. Glu72^{Nuf2} is not conserved (Figure S6), is exposed, does not contact Ndc80, and is not part of the microtubule-binding interface. Glu72Gly and wild-type Ndc80^{bonsai} bind microtubules with indistinguishable affinity (Figure S2). Ndc80$^{\Delta N\text{-bonsai}}$ (7 mg/ml) was crystallized by sitting drop vapor diffusion using a Honeybee Cartesian robot and 96-well plates. Diffraction-quality crystals were obtained by optimizing the initial conditions in hanging drops. The optimal reservoir buffer contained 4.5%–6.5% PEG 6000, 1.5%–2% MPD, 100 mM HEPES, pH 7.5, 16 mM TCEP, and 15 mM phenol. A selenomethionine (SeMet) derivative of the complex was crystallized under similar conditions. Crystals were improved by microseeding, crushing initial crystals with a cat whisker, and seeding with this whisker drops that had been equilibrated for 0.5–1 hr against a standard reservoir solution (see above), with protein concentrations of 7–10 mg/ml. Crystals were transferred to cryobuffer containing the reservoir liquor supplemented with 17.5%–22% glycerol and flash frozen in liquid nitrogen. X-ray diffraction data from single crystals were collected at the European Synchrotron Radiation Facility (Grenoble, France) at beamlines BM16 (SeMet crystal) and ID23-1 (native crystal). X-ray diffraction data were processed with HKL2000 (Otwinowski and Minor, 1997). Two copies of the CH domain of Ndc80 (Wei et al., 2007) in the asymmetric unit were located by molecular replacement with Phaser (McCoy et al., 2007). The resulting electron density maps were too noisy to locate the rest of the molecule. We solved the substructure of 33 of the 36 Se sites in the asymmetric unit of the SeMet derivative. Initial SAD phases were calculated using SHELXD in hkl2map and SHARP (Pape and Schneider, 2004; Vonrhein et al., 2006) for solvent flattening and density modification and further improved with Pirate (Cowtan, 2000). Model building was carried out in Coot (Emsley and Cowtan, 2004), with the help of fragments built automatically with the helical recognition module of ARP/wARP (Morris et al., 2004) and Buccaneer (Cowtan, 2006). Model refinement was carried out with the CNS suite (Brunger et al., 1998) and with Refmac (Murshudov et al., 1997). The Collaborative Computational Project, Number 4 suite (CCP4, 1994) was also used at several stages. The structure was illustrated with PyMOL (DeLano Scientific LLC).

Microtubule-Binding Assay with the Fluorescent Ndc80 Complex, Cosedimentation Assay, Microinjection Experiments, and Electron Microscopy

See Supplemental Experimental Procedures.

ACCESSION NUMBERS

The Protein Data Bank (PDB) ID code of $Ndc80^{\Delta N\text{-}bonsai}$ is 2VE7.

SUPPLEMENTAL DATA

Supplemental Data include Supplemental Experimental Procedures, Supplemental Discussion, eight figures, and one table and can be found with this article online at http://www.cell.com/cgi/content/full/133/3/427/DC1/.

ACKNOWLEDGMENTS

We thank the staff at ESRF for assistance in data collection, V. Cecatiello for assistance in crystallization, and the Musacchio group for discussions. A.M. is funded by the Association for International Cancer Resarch (AICR), the Telethon Foundation, the EU FP6 program contracts 3D-Repertoire and Mitocheck, the Italian Association for Cancer Research (AIRC), the Fondo di Investimento per la Ricerca di Base (FIRB), and the Italian Ministry of Health. S.P. is a FIRC Postdoctoral Fellow and former EMBO postdoctoral fellow. C.C. dedicates this work to the memory of his father Raffaele.

Received: October 1, 2007
Revised: February 6, 2008
Accepted: March 20, 2008
Published: May 1, 2008

REFERENCES

Bharadwaj, R., Qi, W., and Yu, H. (2004). Identification of two novel components of the human NDC80 kinetochore complex. J. Biol. Chem. *279*, 13076–13085.

Brunger, A.T., Adams, P.D., Clore, G.M., DeLano, W.L., Gros, P., Grosse-Kunstleve, R.W., Jiang, J.S., Kuszewski, J., Nilges, M., Pannu, N.S., et al. (1998). Crystallography & NMR system: A new software suite for macromolecular structure determination. Acta Crystallogr. D Biol. Crystallogr. *54*, 905–921.

Cassimeris, L., and Spittle, C. (2001). Regulation of microtubule-associated proteins. Int. Rev. Cytol. *210*, 163–226.

Castresana, J., and Saraste, M. (1995). Does Vav bind to F-actin through a CH domain? FEBS Lett. *374*, 149–151.

Cheeseman, I.M., and Desai, A. (2008). Molecular architecture of the kinetochore-microtubule interface. Nat. Rev. Mol. Cell Biol. *9*, 33–46.

Cheeseman, I.M., Chappie, J.S., Wilson-Kubalek, E.M., and Desai, A. (2006). The conserved KMN network constitutes the core microtubule-binding site of the kinetochore. Cell *127*, 983–997.

Ciferri, C., De Luca, J., Monzani, S., Ferrari, K.J., Ristic, D., Wyman, C., Stark, H., Kilmartin, J., Salmon, E.D., and Musacchio, A. (2005). Architecture of the human ndc80-hec1 complex, a critical constituent of the outer kinetochore. J. Biol. Chem. *280*, 29088–29095.

Ciferri, C., Musacchio, A., and Petrovic, A. (2007). The Ndc80 complex: Hub of kinetochore activity. FEBS Lett. *581*, 2862–2869.

Cimini, D., Wan, X., Hirel, C.B., and Salmon, E.D. (2006). Aurora kinase promotes turnover of kinetochore microtubules to reduce chromosome segregation errors. Curr. Biol. *16*, 1711–1718.

Cleveland, D.W., Mao, Y., and Sullivan, K.F. (2003). Centromeres and kinetochores: from epigenetics to mitotic checkpoint signaling. Cell *112*, 407–421.

CCP4 (Collaborative Computational Project, Number 4) (1994). The CCP4 suite: programs for protein crystallography. Acta Crystallogr. D Biol. Crystallogr. *50*, 760–763.

Cowtan, K. (2000). General quadratic functions in real and reciprocal space and their application to likelihood phasing. Acta Crystallogr. D Biol. Crystallogr. *56*, 1612–1621.

Cowtan, K. (2006). The Buccaneer software for automated model building. 1. Tracing protein chains. Acta Crystallogr. D Biol. Crystallogr. *62*, 1002–1011.

de Arruda, M.V., Watson, S., Lin, C.S., Leavitt, J., and Matsudaira, P. (1990). Fimbrin is a homologue of the cytoplasmic phosphoprotein plastin and has domains homologous with calmodulin and actin gelation proteins. J. Cell Biol. *111*, 1069–1079.

DeLuca, J.G., Dong, Y., Hergert, P., Strauss, J., Hickey, J.M., Salmon, E.D., and McEwen, B.F. (2005). Hec1 and nuf2 are core components of the kinetochore outer plate essential for organizing microtubule attachment sites. Mol. Biol. Cell *16*, 519–531.

DeLuca, J.G., Gall, W.E., Ciferri, C., Cimini, D., Musacchio, A., and Salmon, E.D. (2006). Kinetochore microtubule dynamics and attachment stability are regulated by Hec1. Cell *127*, 969–982.

Dong, Y., Vanden Beldt, K.J., Meng, X., Khodjakov, A., and McEwen, B.F. (2007). The outer plate in vertebrate kinetochores is a flexible network with multiple microtubule interactions. Nat. Cell Biol. *9*, 516–522.

Dougherty, G.W., Adler, H.J., Rzadzinska, A., Gimona, M., Tomita, Y., Lattig, M.C., Merritt, R.C., Jr., and Kachar, B. (2005). CLAMP, a novel microtubule-associated protein with EB-type calponin homology. Cell Motil. Cytoskeleton *62*, 141–156.

Emsley, P., and Cowtan, K. (2004). Coot: model-building tools for molecular graphics. Acta Crystallogr. D Biol. Crystallogr. *60*, 2126–2132.

Foltz, D.R., Jansen, L.E., Black, B.E., Bailey, A.O., Yates, J.R., and Cleveland, D.W. (2006). The human CENP-A centromeric nucleosome-associated complex. Nat. Cell Biol. *8*, 458–469.

Furuyama, S., and Biggins, S. (2007). Centromere identity is specified by a single centromeric nucleosome in budding yeast. Proc. Natl. Acad. Sci. USA *104*, 14706–14711.

Gillett, E.S., Espelin, C.W., and Sorger, P.K. (2004). Spindle checkpoint proteins and chromosome-microtubule attachment in budding yeast. J. Cell Biol. *164*, 535–546.

Gimona, M., Djinovic-Carugo, K., Kranewitter, W.J., and Winder, S.J. (2002). Functional plasticity of CH domains. FEBS Lett. *513*, 98–106.

Hayashi, I., and Ikura, M. (2003). Crystal structure of the amino-terminal microtubule-binding domain of end-binding protein 1 (EB1). J. Biol. Chem. *278*, 36430–36434.

Hori, T., Haraguchi, T., Hiraoka, Y., Kimura, H., and Fukagawa, T. (2003). Dynamic behavior of Nuf2-Hec1 complex that localizes to the centrosome and centromere and is essential for mitotic progression in vertebrate cells. J. Cell Sci. *116*, 3347–3362.

Joglekar, A.P., Bouck, D.C., Molk, J.N., Bloom, K.S., and Salmon, E.D. (2006). Molecular architecture of a kinetochore-microtubule attachment site. Nat. Cell Biol. *8*, 581–585.

Kline-Smith, S.L., Sandall, S., and Desai, A. (2005). Kinetochore-spindle microtubule interactions during mitosis. Curr. Opin. Cell Biol. *17*, 35–46.

Korenbaum, E., and Rivero, F. (2002). Calponin homology domains at a glance. J. Cell Sci. *115*, 3543–3545.

Krissinel, E., and Henrick, K. (2007). Inference of macromolecular assemblies from crystalline state. J. Mol. Biol. *372*, 774–797.

Liu, S.T., Rattner, J.B., Jablonski, S.A., and Yen, T.J. (2006). Mapping the assembly pathways that specify formation of the trilaminar kinetochore plates in human cells. J. Cell Biol. *175*, 41–53.

Maiato, H., DeLuca, J., Salmon, E.D., and Earnshaw, W.C. (2004). The dynamic kinetochore-microtubule interface. J. Cell Sci. *117*, 5461–5477.

Maiolica, A., Cittaro, D., Borsotti, D., Sennels, L., Ciferri, C., Tarricone, C., Musacchio, A., and Rappsilber, J. (2007). Structural analysis of multi-protein complexes by cross-linking, mass spectrometry and database searching. Mol. Cell. Proteomics *6*, 2200–2211.

McAinsh, A.D., Tytell, J.D., and Sorger, P.K. (2003). Structure, function, and regulation of budding yeast kinetochores. Annu. Rev. Cell Dev. Biol. *19*, 519–539.

McCleland, M.L., Kallio, M.J., Barrett-Wilt, G.A., Kestner, C.A., Shabanowitz, J., Hunt, D.F., Gorbsky, G.J., and Stukenberg, P.T. (2004). The vertebrate Ndc80 complex contains Spc24 and Spc25 homologs, which are required to establish and maintain kinetochore-microtubule attachment. Curr. Biol. *14*, 131–137.

McCoy, A.J., Grosse-Kunstleve, R.W., Adams, P.D., Winn, M.D., Storoni, L.C., and Read, R.J. (2007). Phaser crystallographic software. J. Appl. Cryst. *40*, 658–674.

Meraldi, P., McAinsh, A.D., Rheinbay, E., and Sorger, P.K. (2006). Phylogenetic and structural analysis of centromeric DNA and kinetochore proteins. Genome Biol. *7*, R23.

Morris, R.J., Zwart, P.H., Cohen, S., Fernandez, F.J., Kakaris, M., Kirillova, O., Vonrhein, C., Perrakis, A., and Lamzin, V.S. (2004). Breaking good resolutions with ARP/wARP. J. Synchrotron Radiat. *11*, 56–59.

Murshudov, G.N., Vagin, A.A., and Dodson, E.J. (1997). Refinement of macromolecular structures by the maximum-likelihood method. Acta Crystallogr. D Biol. Crystallogr. *53*, 240–255.

Musacchio, A., and Salmon, E.D. (2007). The spindle-assembly checkpoint in space and time. Nat. Rev. Mol. Cell Biol. *8*, 379–393.

Nousiainen, M., Sillje, H.H., Sauer, G., Nigg, E.A., and Korner, R. (2006). Phosphoproteome analysis of the human mitotic spindle. Proc. Natl. Acad. Sci. USA *103*, 5391–5396.

O'Connell, C.B., and Khodjakov, A.L. (2007). Cooperative mechanisms of mitotic spindle formation. J. Cell Sci. *120*, 1717–1722.

Okada, M., Cheeseman, I.M., Hori, T., Okawa, K., McLeod, I.X., Yates, J.R., Desai, A., and Fukagawa, T. (2006). The CENP-H-I complex is required for the efficient incorporation of newly synthesized CENP-A into centromeres. Nat. Cell Biol. *8*, 446–457.

Otwinowski, Z., and Minor, W. (1997). Processing of X-ray diffraction data collected in oscillation mode. In Methods in Enzymology, Volume 276: Macromolecular Crystallography, part A,, C.W. Carter, Jr. and R.M. Sweet, eds. (New York: Academic Press), pp. 307–326.

Pape, T., and Schneider, T.R. (2004). HKL2MAP: a graphical user interface for phasing with SHELX programs. J. Appl. Cryst. *37*, 843–844.

Sandblad, L., Busch, K.E., Tittmann, P., Gross, H., Brunner, D., and Hoenger, A. (2006). The Schizosaccharomyces pombe EB1 homolog Mal3p binds and stabilizes the microtubule lattice seam. Cell *127*, 1415–1424.

Serber, Z., and Ferrell, J.E., Jr. (2007). Tuning bulk electrostatics to regulate protein function. Cell *128*, 441–444.

Sessa, F., Mapelli, M., Ciferri, C., Tarricone, C., Areces, L.B., Schneider, T.R., Stukenberg, P.T., and Musacchio, A. (2005). Mechanism of Aurora B activation by INCENP and inhibition by Hesperadin. Mol. Cell *18*, 379–391.

Slep, K.C., and Vale, R.D. (2007). Structural basis of microtubule plus end tracking by XMAP215, CLIP-170, and EB1. Mol. Cell *27*, 976–991.

Tanaka, T.U., Stark, M.J., and Tanaka, K. (2005). Kinetochore capture and bi-orientation on the mitotic spindle. Nat. Rev. Mol. Cell Biol. *6*, 929–942.

Vonrhein, C., Blanc, E., Roversi, P., and Bricogne, G. (2006). Automated structure solution with autoSHARP. Methods Mol. Biol. *364*, 215–230.

Waterman-Storer, C.M., and Salmon, E.D. (1998). How microtubules get fluorescent speckles. Biophys. J. *75*, 2059–2069.

Wei, R.R., Sorger, P.K., and Harrison, S.C. (2005). Molecular organization of the Ndc80 complex, an essential kinetochore component. Proc. Natl. Acad. Sci. USA *102*, 5363–5367.

Wei, R.R., Schnell, J.R., Larsen, N.A., Sorger, P.K., Chou, J.J., and Harrison, S.C. (2006). Structure of a central component of the yeast kinetochore: the Spc24p/Spc25p globular domain. Structure *14*, 1003–1009.

Wei, R.R., Al-Bassam, J., and Harrison, S.C. (2007). The Ndc80/HEC1 complex is a contact point for kinetochore-microtubule attachment. Nat. Struct. Mol. Biol. *14*, 54–59.